Full Paper
doi.org/10.1002/chem.202001818


Enzyme Models

# Enhancing Tris(pyrazolyl)borate-Based Models of Cysteine/Cysteamine Dioxygenases through Steric Effects: Increased Reactivities, Full Product Characterization and Hints to Initial Superoxide Formation

Lars Müller, Santina Hoof, Matthias Keck, Christian Herwig, and Christian Limberg*[a]

**Abstract:** The design of biomimetic model complexes for the cysteine dioxygenase (CDO) and cysteamine dioxygenase (ADO) is reported, where the 3-His coordination of the iron ion is simulated by three pyrazole donors of a trispyrazolyl borate ligand (Tp) and protected cysteine and cysteamine represent substrate ligands. It is found that the replacement of phenyl groups—attached at the 3-positions of the pyrazole units in a previous model—by mesityl residues has massive consequences, as the latter arrange to a more spacious reaction pocket. Thus, the reaction with $O_2$ proceeds much faster and afterwards the first structural characterization of an iron(II) $\eta^2$-*O*,*O*-sulfinate product became possible. If one of the three Tp-mesityl groups is placed in the 5-position, an even larger reaction pocket results, which leads to yet faster rates and accumulation of a reaction intermediate at low temperatures, as shown by UV/Vis and Mössbauer spectroscopy. After comparison with the results of investigations on the cobalt analogues this intermediate is tentatively assigned to an iron(III) superoxide species.

## Introduction

$O_2$-activating nonheme iron enzymes continue to attract significant attention as they can catalyze oxygenation reactions with high efficiency and selectivity, the realization of which in chemical laboratories would be highly desirable.[1] Hence, many researchers aim at constructing artificial low-molecular weight analogues for these enzymes, that is, biomimetic model complexes, which mimic their structural or functional characteristics, for two main reasons: Firstly, such models can, for instance, provide insights in how far selected structural features that characterize a certain active site are essential for the enzymes' function and thus have to be considered in the development of bioinspired catalysts. Secondly, they can contribute to a mechanistic understanding of the substrate conversion mediated by the enzyme and thus allow progress in the area of biological understanding.[2]

Within the family of nonheme iron oxygenases there are two structural varieties, namely dinuclear and mononuclear representatives. The latter group is divided into monoxygenases and dioxygenases.[3] Among the dioxygenases most members feature a single iron atom coordinated by two histidine donors and one amino acid derived carboxylate function in a typical 2-His/1-Asp(Glu) facial orientation.[1] However, a smaller number of dioxygenases contain an iron center that is coordinated exclusively by three histidine residues.[4] The first enzyme of that type, for which a structural characterization was achieved is the enzyme cysteine dioxygenase (CDO).[5] It catalyzes the reaction between cysteinate and dioxygen to yield cysteine sulfinic acid (see Scheme 1), which lies at the branching point of cysteine catabolism (leading either to sulfate or taurine), and functions to maintain acceptable levels of cysteine in the body.[5]

To gain insight into the effects of the metal–ligand coordination environment, several groups, including us,[6–10] have pursued the creation of synthetic model complexes that mimic the active site of CDO enzymes, which is challenging, since iron oxidation instead of S-oxygenation as well as overoxidation at the S atom has to be avoided. Hence, often selected aspects of structure or function were in the focus. Ligand spheres differing from the facial 3-N coordination environment characteristic for CDO enzymes and thiolates distinguished

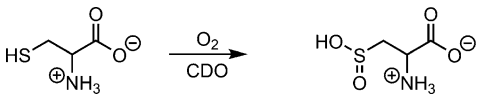


**Scheme 1.** Initial dioxygenation of cysteine by dioxygen in the catabolism of cysteine by CDO.

[a] *L. Müller, S. Hoof, M. Keck, C. Herwig, Prof. Dr. C. Limberg*
*Institut für Chemie, Humboldt-Universität zu Berlin*
*Brook-Taylor-Straße 2, 12489 Berlin (Germany)*
*E-mail: christian.limberg@chemie.hu-berlin.de*

*Supporting information and the ORCID identification number(s) for the author(s) of this article can be found under: https://doi.org/10.1002/chem.202001818.*

from the natural substrates (partly tethered to the N donor framework) were employed to learn what key (structural, electronic) features influence properties and control reactivity.

In this context, we have designed mimics of the CDO active site[7,8] using the trispyrazolyl borate ligand (Tp), which we have found well suited also for the development of replicates of other $(His)_3Fe$ dioxygenases;[10–12] the facial arrangement of three pyrazole donors, albeit charged, is reminiscent of the three histidine-derived imidazole donors.[10] Hence, using a Tp ligand it indeed proved possible to create a structural and functional model of the CDO-substrate complex (CDO-Cys), namely [$Tp^{Ph,Me}$FeCysOEt], **1 a** (CysOEt = L-cysteine ethyl ester) (Scheme 2).[7] Similarly to the structure of CDO-Cys also in the model **1 a** a (protected) cysteinate unit is found as a chelating ligand at the iron(II) center and treatment with dioxygen leads to dioxygenase activity and a sulfinato complex, for which a strong resemblance to the product complex of the CDO was inferred. The results of both density functional theory (DFT) calculations as well as X-ray absorption near edge structure (XANES) and extended X-ray absorption fine structure (EXAFS) measurements, suggested a binding of the formed sulfinate in the dioxygenation product [$Tp^{Ph,Me}Fe(O_2S\text{-}CH_2\text{-}CH\text{-}NH_2)(CO_2Et)$], **2 a**, in an $\eta^2$-*O*,*O*-binding mode[8] similarly to the biological system, for which this specific binding mode was predicted by DFT calculations (Scheme 2).[13] This underlines the excellent model character of complex **1 a**.

In analogy to the model for the CDO **1 a** a possible model compound for the cysteamine dioxygenase (ADO) [$Tp^{Ph,Me}$FeCysAm], **1 b** (CysAm = cysteamine) was synthesized with bound cysteamine instead of L-cysteine ethyl ester.[17] Also this complex reacts with dioxygen, yielding the product [$Tp^{Ph,Me}Fe(O_2S\text{-}CH_2\text{-}CH_2\text{-}NH_2)$], **2 b**. After acidic workup the oxidation product could be isolated and identified as hypotaurine, based on the results from electrospray ionization (ESI) mass spectrometry and $^1H$ NMR spectroscopy.[17]

DFT calculations on the mechanism of the CDO model reaction revealed that various intermediates occur with only low activation barriers between them, so that they eluded isolation, and in all of them one of the pyrazole donors for steric reasons was found to be released from the metal center.[8] Contemplating a further optimization of this model we then decided to employ a Tp ligand derivative, where the phenyl residues in **1 a** and **1 b** are replaced by mesityl residues. We anticipated that the protective pocket would lead to a stabilization and thus further characterization of intermediates and/or final products. Here we report our results.

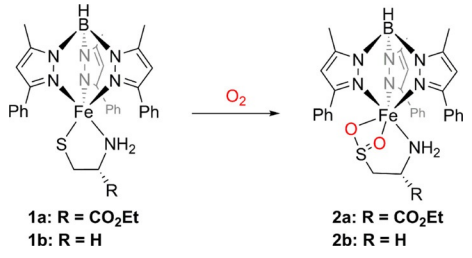


**Scheme 2.** Dioxygenation of [$Tp^{Ph,Me}$FeCysOEt], **1 a**, and [$Tp^{Ph,Me}$FeCysAm], **1 b**, to [$Tp^{Ph,Me}Fe(O_2S\text{-}CH_2\text{-}CH\text{-}NH_2)(CO_2Et)$], **2 a**, and [$Tp^{Ph,Me}Fe(O_2S\text{-}CH_2\text{-}CH_2\text{-}NH_2)$], **2 b**, respectively.

## Results and Discussion

### Synthesis and investigation of precursor complexes

The potassium salts of the ligands [$Tp^{Mes}$]$^-$ ($Tp^{Mes}$ = hydrotris(3-mesitylpyrazol-1-yl)borate, see Scheme 3) and [$Tp^{Mes*}$]$^-$ ($Tp^{Mes*}$ = hydrobis-(3-mesitylpyrazol-1-yl)(5-mesitylpyrazol-1-yl)-borate, see Scheme 3), were synthesized as described by Trofimenko and co-workers, who separated the thallium salts Tl[$Tp^{Mes}$], **II**, and Tl[$Tp^{Mes*}$], **II′**, by fractionalized crystallization.[14] $Tp^{Mes*}$—the first example of an asymmetric Tp ligand—was formed independently of the reaction conditions as the main product. To avoid the use of toxic thallium salts we utilized the potassium salts, which we were able to separate by fractionalized crystallization, leading to the ether adduct $(Et_2O)$K[$Tp^{Mes}$], **I**, and K[$Tp^{Mes*}$], **I′**.

Both potassium salts were subjected to a salt metathesis with iron(II) chloride, which gave complexes [$Tp^{Mes}$FeCl], **3**, and [$Tp^{Mes*}$FeCl], **3′**, in good yields of 77 and 84%, respectively. Single crystals of the complexes **3** and **3′** were grown by layering a concentrated dichloromethane (DCM) solution with acetonitrile (MeCN). The spectroscopic and crystallographic data reveal bond lengths and angles that correspond to those of other $Tp^{Mes}$MX and $Tp^{Mes*}$MX derivatives (M = transition metal, X = halogen) reported in the literature.[14–16,18] Due to the steric bulk of the three mesityl substituents oriented facially in complex **3**, a coordination by three pyrazole N atoms and one chlorido ligand results (see Supporting Information, Figure S1). In contrast to this, complex **3′** crystallized as [$Tp^{Mes*}$Fe(NCMe)Cl], **3′·MeCN**, where in addition to the three pyrazole N atoms and the chlorido ligand one acetonitrile molecule coordinates to the iron atom (see Supporting Information, Figure S1). This additional solvent molecule can be easily removed by applying vacuum conditions to regain the solvent free complex **3′**.

The target complexes [$Tp^{Mes}$FeCysOEt], **4 a**, [$Tp^{Mes}$FeCysAm], **4 b**, and [$Tp^{Mes*}$FeCysAm], **4′b**, were synthesized in excellent yields of more than 90% from the respective complexes **3** and **3′** by reaction with the respective thiols in the presence of $Et_3N$ (Scheme 4).

Single crystals of compounds **4 a** and **4 b** were grown by slow evaporation of the volatiles from a benzene or toluene solution and the results of X-ray diffraction analyses are shown

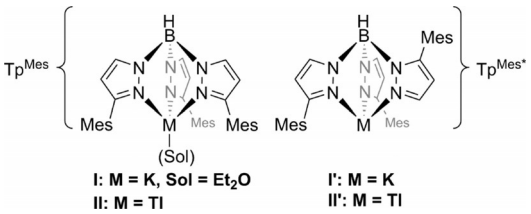


**Scheme 3.** Symmetric ligand precursor M[$Tp^{Mes}$](·Sol), **I** (M = K, Sol = $Et_2O$), **II** (M = Tl) and asymmetric ligand precursor M[$Tp^{Mes*}$], **I′** (M = K), **II′** (M = Tl).

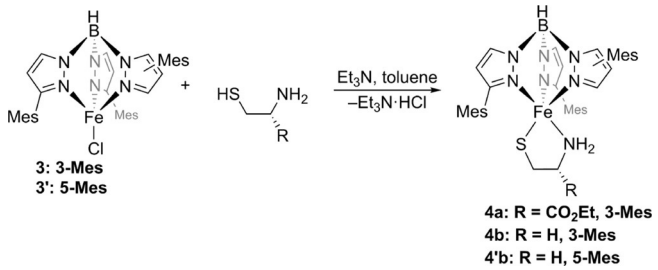


**Scheme 4.** Synthesis of the target complexes [Tp$^{Mes}$FeCysOEt], **4a**, [Tp$^{Mes}$FeCysAm], **4b**, and [Tp$^{Mes}$*FeCysAm], **4'b**.

in Figure 1a and b. The bond angles and lengths found for **4a** and **4b** are in good agreement with those of complexes **1a** and **1b** published earlier; details can be found in the Supporting Information (Table S1).

As in the structure of the substrate complex of CDO the cysteinato unit in **4a** binds as a chelating ligand, so that the immediate coordination spheres of the iron centers in the CDO and in **4a** are very similar. The iron(II) ion in **4a** is coordinated by the three nitrogen atoms of the Tp$^{Ph,Me}$ ligand as well as by the amine and thiolate functions of the S-deprotonated cysteine ethyl ester in a geometric arrangement that is in-between trigonal bipyramidal and square pyramidal. The $\tau$ parameter differs with $\tau = 0.50$ somewhat from the one of **1a** ($\tau = 0.68$),[7] and both are comparable to those reported for CDO enzymes, which range between 0.46[5e] and 0.71[5d] (structures for the ADO are not available yet); with $\tau = 0.45$ **4b** features an even smaller value than **4a** and again the one observed with Tp$^{Ph,Me}$ was significantly higher (**1b**, $\tau = 0.57$).[17] Hence, the replacement of Tp$^{Ph,Me}$ by Tp$^{Mes}$ leads to some transformation from trigonal bipyramidal towards square planar and thus to somewhat more open vacant coordination sites for the potential binding and activation of dioxygen. A closer inspection and comparison of the structures in this regard revealed a consequential phenomenon: While seemingly the replacement of phenyl by mesityl leads to an increased steric bulk around the metal center, in fact the mesityl units—unlike the phenyl residues—arrange themselves to a cup (Figures 2a and b), forming counterintuitively a more spacious reaction pocket around the metal center as compared to Tp$^{Ph,Me}$. Naturally, this is relevant for the reactivity described below and the observation was also corroborated by topographic steric maps, which were constructed based on the X-ray diffraction data of the complexes **1a**, **1b**, **4a** and **4b** using the web application SambVca 2.1.[19] For better clarity only the Tp ligands are visualized and the substrate ligands cysteinate and cysteaminate omitted. The cup-like arrangement of the mesityl residues belonging to the Tp$^{Mes}$ ligand are well visible in the steric maps of complexes **4a** and **4b** (Figure 2d, Figure S4d). By contrast, the steric maps of complexes **1a** and **1b** visualize, that at least in the solid state the phenyl residues reach into the space around the iron center (Figure 2c, Figure S4 c)).

Apart from X-ray diffraction, compounds **4a**, **4b** and **4'b** were characterized by ESI-MS, NMR spectroscopy, magnetic measurements (Evans method) and IR spectroscopy. As expected from the previous results,[8] they were found to have high-spin configurations and in the attenuated total reflection infrared (ATR-IR) spectra besides a band caused by the characteris-

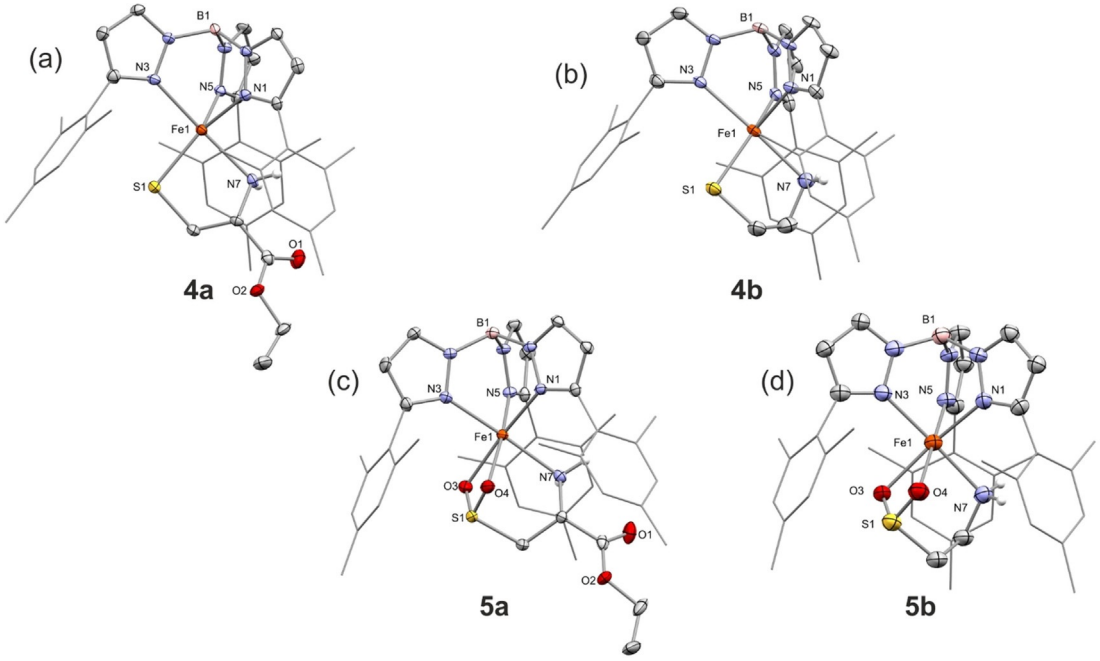


**Figure 1.** Molecular structures of **4a**, **4b**, **5a** and **5b** as determined by single crystal XRD. a) [Tp$^{Mes}$FeCysOEt], **4a**, selected bond lengths [in Å]: Fe1–N7 2.244(4), Fe1–S1 2.2874(13); b) [Tp$^{Mes}$FeCysAm], **4b**, selected bond lengths [in Å]: Fe1–N7 2.252(3), Fe1–S1 2.3202(7); c) [Tp$^{Mes}$Fe($O_2$S-$CH_2$-CH-$NH_2$)($CO_2$Et)], **5a**, selected bond lengths [in Å] and angles [in °]: Fe1–N7 2.252(3), Fe1–O3 2.149(2), Fe1–O4 2.209(2), S1–O3 1.524(2), S1–O4 1.520(2), O3-S1-O4 104.91(12); d) [Tp$^{Mes}$Fe($O_2$S-$CH_2$-$CH_2$-$NH_2$)], **5b**, selected bond lengths [in Å] and angles [in °]: Fe1–N7 2.225(6), Fe1–O3 2.224(5), Fe1–O4 2.186(5), S1–O3 1.537(6), S1–O4 1.537(6), O3-S1-O4 105.37(3), based on single-crystal X-ray diffraction, solvent of crystals and hydrogen atoms omitted except $NH_2$.

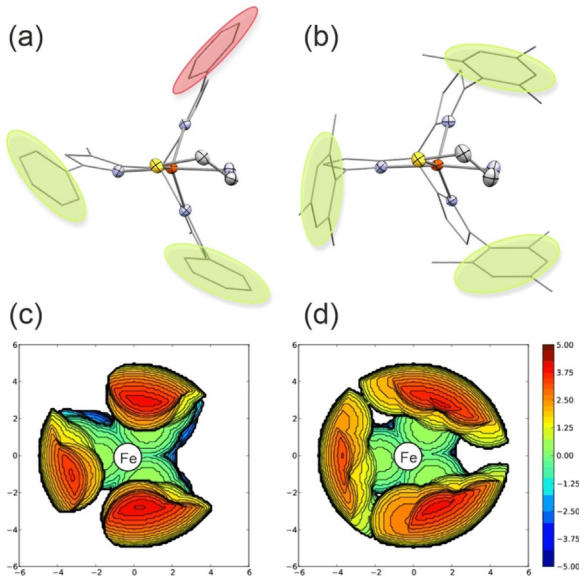


**Figure 2.** Molecular structures of a) [Tp$^{Ph,Me}$FeCysAm], **1b**, revealing that in the solid state a phenyl residue is reaching into the space around the iron center, b) [Tp$^{Mes}$FeCysAm], **4b**, with mesityl residues arranging themselves to a cup. Topographic steric maps of c) [Tp$^{Ph,Me}$FeCysAm], **1b**, and d) [Tp$^{Mes}$FeCysAm], **4b**, with a sphere diameter of 5 Å shown in the same orientation as molecular structures above, leaving out the substrate ligands cysteine ethyl ester and cysteamine.

tic vibrations of the B–H bonds at around 2450 cm$^{-1}$ two further characteristic vibrational absorptions at around 3360 and 3280 cm$^{-1}$ appear, which can be attributed to the amino functions now present in the compounds. Additionally, the ester function of complex **4a** shows a characteristic vibration at 1727 cm$^{-1}$.

### Reaction with $O_2$ and product analysis

$^1$H NMR spectroscopic studies showed that complexes **4a**, **4b** and **4'b** react with dioxygen readily within minutes, while for complexes **1a** and **1b** complete dioxygenation was observed only after 14 hours.[7,17] The clear solutions of the products resulting from the reactions of **4a** and **4b**, which were conceivable to correspond to [Tp$^{Mes}$Fe(O$_2$S-CH$_2$-CH$_2$-NH$_2$)(CO$_2$Et)], **5a**, and [Tp$^{Mes}$Fe(O$_2$S-CH$_2$-CH$_2$-NH$_2$)], **5b**, remained colorless for extended periods of time under an oxygen atmosphere. In the case of **4'b** the solution changed color to light orange within several minutes indicating a further reaction of the initially formed [Tp$^{Mes}$*Fe(O$_2$S-CH$_2$-CH$_2$-NH$_2$], **5'b**, with dioxygen. The drastically increased reactivity of **4a** and **4b** compared to **1a** and **1b** may be rationalized on the basis of the solid-state structures. As pointed out above, the reaction pockets of **4a** and **4b** were found to offer more space, and if the solid state structures reflect a preferred situation also in solution, this explains the acceleration of the so far quite slow reactions. At the same time, the increased size of the pocket in combination with the increased bulk of the residues also leads to a higher degree of protection: unlike in the case of the sulfinate complexes **2a** and **2b**, which were too unstable to grow crystals for an XRD study, upon replacement of the phenyl by mesityl substituents the products of the $O_2$ reaction were sufficiently stable to be crystallized from benzene and the result of X-ray structure analysis supported the assumed identities of **5a** and **5b** (Figure 1c and d). The iron(II) atoms are coordinated pseudo-octahedrally by three nitrogen atoms of the Tp ligand, one amino function of the substrate and the sulfinate function in an $\eta^2$-*O,O*-coordination mode. The latter had been inferred before for complexes **2a** and **2b** based on DFT calculations and EXAFS measurements[11] and is thought to also represent the binding mode in the biological system.[13] The solid-state structures of **5a** and **5b** thus confirm the earlier suggestions and are in fact the first iron(II)-sulfinate structures featuring the $\eta^2$-*O,O*-binding mode, which could be characterized by single-crystal XRD (for CDO models investigated by Goldberg and co-workers $\eta^1$-*S*-binding had been found).[6b] The sulfur-oxygen bonds are almost identical in length within **5a** (S1–O3: 1.524(2), S1–O4: 1.520(2) Å) and identical within complex **5b** (S1–O3, S1–O4: 1.537(6) Å), respectively. However, within each of the complexes the iron oxygen bonds are slightly different (**5a**: Fe1–O3: 2.224(5), Fe1–O4: 2.186(5) Å; **5b**: Fe1–O3: 2.149(2), Fe1–O4: 2.209(2) Å). The oxygen-sulfur-oxygen angles are with 104.91(12) and 105.37(3)° smaller than the expected tetrahedral angle of 109.5°, likely due to the steric demand of the lone pairs at sulfur.

Investigation on the magnetic properties with the aid of the Evans method revealed that—as expected—all product complexes **5a**, **5b** and **5b'** have a $S=2$ high-spin ground state (for further details see Supporting Information).

The ATR-IR spectra of the solid complexes **5a**, **5b** and **5'b** show the characteristic bands of N–H, B–H and C=O vibrations shifted compared with the parent compounds. In addition absorptions in the fingerprint region between 990 and 950 cm$^{-1}$ can be assigned to S=O stretching vibrations.[22,23] Also bands for Fe–O vibrations could be identified between 650 and 480 cm$^{-1}$, which have reasonable intensity in case of complexes **5b** and **5'b**, while those of **5a** are quite weak (Table 1, Figure S8). A detailed analysis of the vibrational modes was performed exemplarily for complex **5b** with the help of DFT calculations (Figure S13, Figure S14). Two asymmetric (979, 934 cm$^{-1}$) and one symmetric S=O vibrations (955 cm$^{-1}$) could be identified as well as two symmetric Fe–O vibrations (532, 482 cm$^{-1}$). Complexes **2b** and **5'b** show similar characteristic patterns in the S=O and Fe–O vibration regions compared to those of **5b**, while the absorptions of **5a** resemble those of

**Table 1.** Symmetric and asymmetric stretching vibrations of the $SO_2$ units bound in the oxygenated products **2b**, [Tp$^{Mes}$Fe(O$_2$S-CH$_2$-CH-NH$_2$)(CO$_2$Et)], **5b**, [Tp$^{Mes}$Fe($^{18}$O$_2$S-CH$_2$-CH$_2$-NH$_2$)], **5b**($^{18}$O), and [Tp$^{Mes}$*Fe(O$_2$S-CH$_2$-CH$_2$-NH$_2$)], **5'b**.

| | $\nu_{as}$(S=O) [cm$^{-1}$] | $\nu_s$(S=O) [cm$^{-1}$] | $\nu_s$(Fe–O) [cm$^{-1}$] |
|---|---|---|---|
| **2b** | 978 | 955 | 529 |
| **5b** | 979, 934 | 955 | 532, 482 |
| **5b**($^{18}$O) | 956 ($\Delta\nu=-23$), 932, 915 ($\Delta\nu=-19$), 899 | – | 516 ($\Delta\nu=-16$), 474 ($\Delta\nu=-8$) |
| **5'b** | 984, 933 | 957 | 532, 481 |

complex **2a**. Reaction with $^{18}O_2$ (99.9%) generated the labeled complexes **5a** ($^{18}O$) and **5b** ($^{18}O$), as confirmed by electrospray ionization mass spectrometry (ESI-MS), which revealed the expected shifts by four units for the [(Tp$^{Mes}$Fe($O_2$S-$CH_2$-CH-$NH_2$)($CO_2$Et))+K]$^+$ peak from *m/z* 842.290 to 846.291 and from *m/z* 770.263 to 774.267 for the [(Tp$^{Mes}$Fe($O_2$S-$CH_2$-$CH_2$-$NH_2$))+K]$^+$ peak (see Figure 3 and Supporting Information, Figure S50). In the IR spectra $^{18}O$-labeling led to a shift of the S=O and Fe–O vibrations to lower wavenumbers for **5a**($^{18}O$) and **5b**($^{18}O$). Exemplarily, in case of complex **5b**($^{18}O$) the two asymmetric vibrations shifted by 23 and 19 $cm^{-1}$ to lower frequencies compared to the non-labeled complex, which fits well to the theoretical shifts as calculated using DFT (20 and 17 $cm^{-1}$, see Supporting Information). The calculations also predicted that the symmetric vibration is replaced by two new asymmetric vibrations, as observed (Table 1). Hence, the insights from the combination of results from single crystal X-ray diffraction and IR spectroscopy for **5a** and **5b** allow for the assignment of the $\eta^2$-*O,O*-binding mode also for complexes for which no single crystals can be grown just based on the IR spectroscopic signature. Accordingly, considering the IR data of **5'b** an analogous binding mode can be inferred, and the IR spectra of **2a** and **2b** now further support $\eta^2$-*O,O*-binding in line with DFT calculations and EXAFS measurements.[8,17]

The mechanisms by which the enzymes and model systems perform the dioxygenation of cysteinate ligands to yield sulfinates have been the subject of various DFT investigations, which led to a consistent picture.[13,24] It is commonly accepted that in the first step of the $O_2$ reaction an iron(III) superoxide species is formed. The distal O atom then attacks at the S atom of the cysteinate ligand, resulting in a structure with a four-membered S-Fe-O-O ring. Subsequently, an O–O bond cleavage occurs to give sulfoxide and an iron(IV) oxido species, which then oxygenates the sulfoxide unit to the sulfinate. Calculations have predicted such a mechanism for the transformation **1a**→**2a**, too,[8] and it is reasonable to assume an analogous proceeding also for the reactions **4**→**5** here.

## Kinetic investigations

After $^1$H NMR spectroscopic experiments had confirmed that the dioxygenation of complexes **4a**, **4b** and **4'b** proceeds much faster than in the case of **1a** and **1b** (see above), temperature-dependent UV/Vis measurements over a range of more than 65 °C were performed. The progress of the reactions was monitored by the decrease of the sulfur-to-iron charge transfer band at around 350 nm in the electronic spectra (see Figures S11–S20). The decay follows a pseudo first-order rate-law in oxygen saturated solvents such as toluene, acetone or dichloromethane. This had already been observed for the complexes **1a**[8] and **1b**[17] as well as for charged complexes featuring $^{Ph2}$TIP as tridentate ligand.[20] The extracted $k_1$ values were plotted in respective Eyring plots to derive thermodynamic constants for each compound (Figure 4, see Supporting Information for further details). Temperature dependent measurements could not be performed with complexes **1a** and **1b**, as temperatures lower than room temperature lead to incomplete reaction and elevated temperatures to product decomposition. Still, the data points at 20 and 25 °C give a good orientation concerning the respective reaction rates.

Although the reaction pathways are expected to be similar for all of the complexes and the oxygenated products are identical in coordination behavior, the reaction rates differ by several orders of magnitude within the studied series. Only a minor influence of the used substrate—either L-cysteine ethyl ester in the complexes **1a** and **4a** vs. cysteamine in the complexes **1b**, **4b** and **4'b**—was found. The complexes with the less sterically demanding cysteamine react only slightly faster than the corresponding L-cysteine ethyl ester complexes. The major influence originates from the employed Tp ligand. The complexes based on Tp$^{Mes}$ react with a factor of 200 faster with dioxygen than the ones based on Tp$^{Ph,Me}$ where the reaction reaches completion only after several hours. Compound **4'b** with the asymmetric ligand Tp$^{Mes*}$ reacts by a factor of two faster than complex **4b**, which is understandable, since even more space is available at the metal center. The Eyring plots show that the activation energies of the rate determining

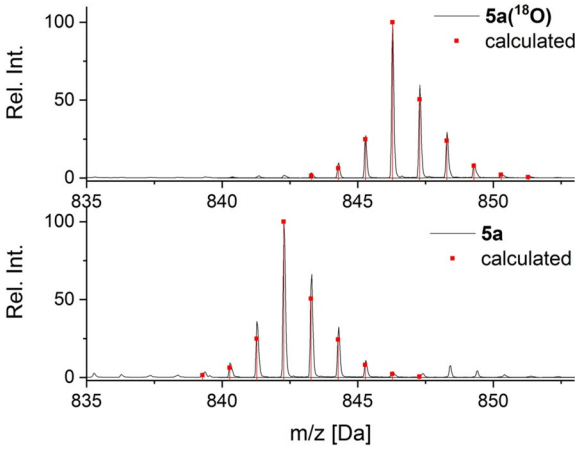


**Figure 3.** [(Tp$^{Mes}$Fe($O_2$S-$CH_2$-$CH_2$-$NH_2$)($CO_2$Et))+K]$^+$ peaks in the ESI-MS of compounds **5a** and **5a**($^{18}O$) in black with calculated pattern in red, normalized to 100%.

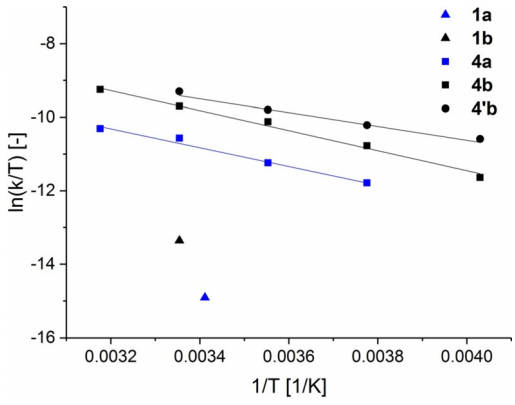


**Figure 4.** Eyring plots of dioxygenation reactions of [Tp$^{Mes}$FeCysOEt], **4a**, [Tp$^{Mes}$FeCysAm], **4b**, and [Tp$^{Mes*}$FeCysAm], **4'b**, and single datapoints for [Tp$^{Ph,Me}$FeCysOEt], **1a**, [Tp$^{Ph,Me}$FeCysAm], **1b**.

steps (rds) of the dioxygenation reactions contain almost no contribution of the entropy, which is close to 0 kcal mol$^{-1}$ K$^{-1}$ in all three cases (Table 2). This indicates that the initial reaction with $O_2$ is not determining the rate. The calculated activation enthalpies are very low between 4 and 6 kcal mol$^{-1}$ for all three dioxygenations; the lowest one is found for the reaction of complex **4'b** to **5'b** with 4.17 kcal mol$^{-1}$. Altogether, these findings also quantitatively confirm that the cup-like arrangement of the mesityl residues and the associated increase in space within the reaction pocket indeed leads to an increase in reaction rates.

**Table 2.** Derived activation parameters for the rate determining steps (rds) of the dioxygenations of [Tp$^{Mes}$FeCysOEt], **4a**, [Tp$^{Mes}$FeCysAm], **4b**, and [Tp$^{Mes}$*FeCysAm], **4'b**.

| Reaction | $\Delta H^{\neq}$ [kcal mol$^{-1}$] | $\Delta S^{\neq} \times 10^{-2}$ [kcal mol$^{-1}$ K$^{-1}$] |
|---|---|---|
| **4a**→**5a** | 5.86 ± 0.36 | −4.87 ± 0.13 |
| **4b**→**5b** | 5.35 ± 0.18 | −4.85 ± 0.07 |
| **4'b**→**5'b** | 4.17 ± 0.37 | −5.19 ± 0.13 |

### Reaction intermediates

When the reaction temperature during the dioxygenation of compound **4'b** was decreased below −40 °C the kinetics could not be determined by monitoring of the sulfur-to-iron charge transfer band at 350 nm anymore, as other absorption bands started to emerge in addition. When the temperature was decreased to −80 °C an intermediate with characteristic absorption maxima at 405, 510 and 645 nm was accumulated (Figure 5). However, this dark purple intermediate, **6'b**, which may represent an iron(III) superoxide species showed at low temperatures, even below −80 °C, a rather short lifetime, which made its isolation impossible.

Similar absorption maxima of 500 and 640 nm in the electronic spectrum, decaying with first-order kinetics, were observed when the enzyme substrate complex of the C164S variant CDO was treated with oxygenated buffer solution in stopped flow experiments, emphasizing the relevance of our study to the biological reaction.[24] Unfortunately, besides Mössbauer spectroscopy no further characterization of the enzymatic intermediate had been possible.

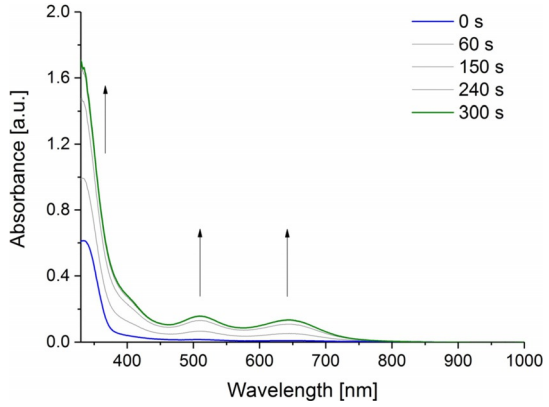


**Figure 5.** UV/Vis spectra showing the generation of the intermediate [Tp$^{Mes}$*Fe(CysAm)($O_2^{-\bullet}$)], **6'b**, from [Tp$^{Mes}$*FeCysAm], **4'b**, (0.4 mM) at −80 °C in oxygen saturated acetone.

Just recently, Kovacs and co-workers reported the generation of an iron(III)-superoxide intermediate upon treatment of [Fe($S_2^{Me2}N_3$(Pr,Pr))] ($S_2^{Me2}N_3$(Pr,Pr) = 2,3,13,14-tetramethyl-2,14-dithiolato-4,8,12-triazapentadeca-3,12-dien) with dioxygen in UV/Vis and resonance Raman experiments at low temperatures showing three comparable maxima in the UV/Vis spectrum (409, 520, 707 nm).[25] Here, the coordination of the iron center by alkyl thiolates resulted in a much more reactive basic superoxide intermediate, which can activate strong C–H bonds but does not perform sulfur oxidation, as it is observed in our studies, emphasizing the importance of the coordination environment for the reaction pathway.

A mixed ligand complex [Tp$^{Me2}$FeL$^{Ph}$] (Tp$^{Me2}$ = hydrotris(3,5-dimethylpyrazol-1-yl) borate, L$^{Ph}$ = methylbis-(1-methylimidazol-2-yl)phenylborate), which is able to bind dioxygen reversibly under formation of an low-spin iron(III) superoxide species was reported by Hikichi and co-workers.[26] This was confirmed by UV/Vis, resonance Raman and $^1$H NMR experiments. The electronic spectrum of this species does not correspond to the one displayed by the intermediate originating from **4'b**, possibly due to the much stronger donating azole L$^{Ph}$ ligand and the resulting $S = 0$ spin state. This superoxide is able to split weak hydrogen-oxygen bonds and can be reduced in a proton-coupled-electron-transfer with decamethyl ferrocene in the presence of a strong acid forming the corresponding hydroperoxo species but no oxygenation of thiols or thiolates was tested.

Fiedler and co-workers published the detection of a Tp iron(III) superoxide intermediate with a coordinated 2-amino thiophenolate substrate ligand (2-ATP).[9b] They observed a dark purple intermediate with absorption maxima in the electronic spectra at 490, 655 and 860 nm upon treatment of [Tp$^{Me2}$Fe(2-ATP)] (Tp$^{Me2}$ = hydrotris(3,5-dimethylpyrazol-1-yl) borate) with dioxygen at −80 °C. The absorption maxima are thus significantly redshifted compared to the absorptions observed in case of **4'b** but have the same characteristic pattern. In contrast to the present study no S-oxygenates but only 2-aminophenyl disulfide was identified as the product of the $O_2$ reaction. To explain its formation an alternative reaction pathway was proposed involving superoxide dissociation and deprotonation of the 2-ATP ligand at the amine function: The higher acidity of the -$NH_2$ donor in 2-ATP compared to cysteine or cysteamine could favor this pathway yielding possibly an iron(III)-amidothiophenolate species before workup.[9b] Altogether, although the reactivity of the abovementioned [Tp$^{Me2}$Fe(2-ATP)$O_2$] differs significantly from the system described in this study, an assignment of the formed intermediate as [Tp$^{Mes}$*Fe(CysAm)($O_2^{-\bullet}$)] (**6'b**) seems reasonable.

Resonance Raman measurements in acetone at −90 °C with 504 nm laser excitation to further support of the identity of the intermediate as a superoxide were unsuccessful, probably due to solubility problems in a concentration range between 5

and 50 mM. However, Mössbauer studies provided further information.

### Mössbauer studies

Mössbauer spectra of complexes **4b** ($\delta = 0.99$ mm s$^{-1}$, $\Delta E_q = 2.79$ mm s$^{-1}$, Supporting Information, Figure S51) and **4'b** ($\delta = 0.96$ mm s$^{-1}$, $\Delta E_q = 3.26$ mm s$^{-1}$, Supporting Information, Figure S52) of the solid samples were measured at 13 K (Figure 6) and the observed resonances are in good agreement with values obtained by Jameson and co-workers for the enzyme substrate complexes of C164S and C93G CDO.[21,24] For both enzyme substrate complexes the signals of two species with similar isomer shifts but differing quadrupole splitting had been observed which was explained by the presence (higher splitting) and absence (lower splitting) of water in the coordination sphere of the iron center in addition to cysteine. Also in the case of **4'b** the occupation of the vacant coordination site by a solvent molecule would explain that the Mössbauer spectrum of **4'b·acetone** in frozen acetone solution has a significantly higher quadrupole splitting compared to the solid sample ($\delta = 0.97$ mm s$^{-1}$, $\Delta E_q = 3.91$ mm s$^{-1}$, Supporting Information, Figure S53) indicating an octahedral coordination of the iron center at least at low temperatures. The addition of acetone[$D_6$] to an NMR sample of **4'b** in $C_6D_6$, however, did not result in changes in the $^1$H NMR spectrum at room temperature. The effect of pentagonal versus octahedral coordination on the quadrupole splitting was also investigated by Goldberg and co-workers by means of the four CDO surrogates [Fe$^{II}$($Me_3$TACN)(abt$^x$)(OTf)] and [Fe$^{II}$($i$Pr$_3$TACN)(abt$^x$)(OTf)] (X = H, $CF_3$, TACN = triazacyclononane, abt = aminobenzene thiolate). The complexes with the less sterically demanding ligand $Me_3$TACN offer enough space for coordination of the triflate ion, resulting in Mössbauer spectra with higher quadrupole splittings ($\delta = 1.07$ mm s$^{-1}$, $\Delta E_q = 3.55$ mm s$^{-1}$, X = H; $\delta = 1.08$ mm s$^{-1}$, $\Delta E_q = 3.20$ mm s$^{-1}$, X = $CF_3$) compared to the complexes with $i$Pr$_3$TACN ligand where no coordination of the triflate ion is possible ($\delta = 0.93$ mm s$^{-1}$, $\Delta E_q = 1.97$ mm s$^{-1}$, X = H; $\delta = 0.95$ mm s$^{-1}$, $\Delta E_q = 2.06$ mm s$^{-1}$, X = $CF_3$).[21] These trends are very well in line with our investigation and support the hypothesis of coordinated acetone to complex **4'b** at low temperatures.

The dioxygenated reaction products **5b** ($\delta = 1.18$ mm s$^{-1}$, $\Delta E_q = 3.43$ mm s$^{-1}$, Supporting Information, Figure S54) and **5'b** ($\delta = 1.08$ mm s$^{-1}$, $\Delta E_q = 3.78$ mm s$^{-1}$, Supporting Information, Figure S55) show similar isomer shifts in the Mössbauer spectra consistent with iron(II) high-spin complexes. The quadrupole splittings are larger than in case of the precursors, due to the $\eta^2$-*O,O*-coordination of the sulfinate. In general, the larger quadrupole splitting of complexes **4'b** and **5'b** compared to **4b** and **5b** are consistent with the more asymmetric Tp$^{Mes*}$ ligand and a therefore less isotropic electron distribution at the iron center. Previous calculations concerning the Mössbauer parameters of enzymatic intermediates and products have shown that this method indeed provides characteristic fingerprints.[24] The signal for the $\eta^2$-*O,O*-bound sulfinate product was predicted to show $\delta = 1.00$ mm s$^{-1}$ and $\Delta E_q = 3.43$ mm s$^{-1}$, which matches the experimental Mössbauer parameters of the products **5b** and **5'b** rather well. Hence, we have used the complex **5b** as a benchmark for the DFT method (B3LYP-D3/TZVP/CP(PPP)) we used to calculate the theoretical Mössbauer resonances of **6'b** (vide infra). Indeed, we observed a very good fit for the $S = 2$ state of **5b** ($\delta = 1.00$ mm s$^{-1}$, $\Delta E_q = 3.67$ mm s$^{-1}$) that had been found experimentally relevant.

The intermediate **6'b** observed in UV/Vis experiments was generated in higher concentrations at −96 °C in acetone for Mössbauer spectroscopic studies (Figure 7), which identified two major species in the frozen reaction mixture.

The starting material **4'b·acetone** was identified with a proportion of 41.2% besides resonances characteristic for an iron(III) species attributed to [Tp$^{Mes*}$Fe(CysAm)($O_2^{\cdot-}$)], **6'b**, with a proportion of 44.3% ($\delta = 0.346$ mm s$^{-1}$, $\Delta E_q = 2.321$ mm s$^{-1}$).

A third resonance with smaller quadrupole splitting and a proportion of 13.5% results from an impurity derived from decomposition during sample handling.

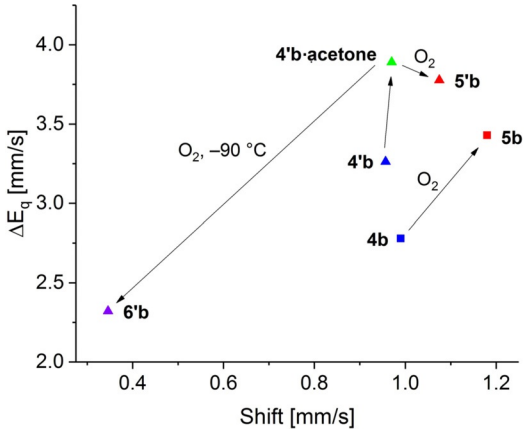


**Figure 6.** Mössbauer shifts and quadrupole splittings determined for complexes **4b**, **4'b**, **5b**, **5'b** in the solid state; complex **4'b** was also investigated in form of a frozen acetone solution and the data of intermediate **6'b** have been derived from frozen acetone reaction mixture.

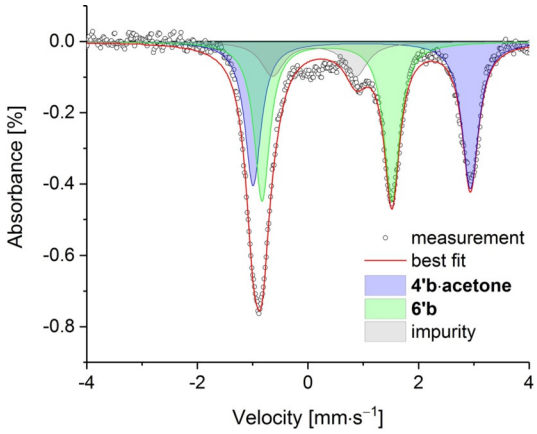


**Figure 7.** Mössbauer spectrum of the frozen mixture generated in the reaction between [Tp$^{Mes*}$FeCysAm], **4'b**, and dioxygen in acetone containing [Tp$^{Mes*}$Fe(CysAm)(acetone)], **4'b·acetone**, and intermediate [Tp$^{Mes*}$Fe(CysAm)($O_2^{\cdot-}$)], **6'b**.

The number of iron(III) superoxide compounds, which have been unequivocally identified as such, is rather small and only few of those have been investigated by Mössbauer studies. Their isomeric shifts are difficult to compare[27] with the one of **6'b** as rather different ligands were employed from case to case and also the spin states vary. Most iron(III) superoxide complexes reported so far have singlet or triplet ground states, for which $\Delta E_q$ values are expected that are larger than in case of an iron(III) high-spin configuration with a symmetric electron distribution. For instance, the quadrupole splitting for a high-spin iron(III) superoxide generated upon treatment of [Fe(BDPP)] (BDPP = 2,6-bis(((*S*)-2-(diphenylhydroxymethyl)-1-pyrrolidinyl) methyl)-pyridine) with dioxygen at −80 °C amounted to 1.65 mm s$^{-1}$ ($\delta$ = 0.58 mm s$^{-1}$) as reported by Chiang et al.[28] By contrast, an intermediate-spin iron(III) complex with a side-on bound superoxide ligand published by Hong et al. showed a $\Delta E_q$ = 2.696 mm s$^{-1}$ ($\delta$ = 0.096 mm s$^{-1}$), which is close to the $\Delta E_q$ of **6'b**.[29] We thus exclude a high-spin configuration **6'b**. To get further insights from theory the Mössbauer parameters of [Tp$^{Mes}$*Fe(CysAm)(O$_2^{-\bullet}$)] were calculated in singlet, triplet and quintet states. The singlet state was found to be significantly higher in energy than the triplet and quintet states, which are almost degenerate. However, only the Mössbauer data calculated for the triplet state matched the experimental data excellently (TZVP/CP(PPP): $\delta$ = 0.36 mm s$^{-1}$, $|\Delta E_q|$ = 2.41 mm s$^{-1}$), while those of the other two states were markedly different.

The Mössbauer spectrum thus supports that the intermediate **6'b** corresponds to a superoxide, to which consequently the three absorption maxima in the electronic spectrum are assigned as well.

### Cobalt analogues

As the intermediate **6'b** was too unstable for isolation, cobalt analogues of complexes **4b** and **4'b** were prepared starting from the blue cobalt chlorido complexes [Tp$^{Mes}$CoCl] (**7**) and [Tp$^{Mes}$*CoCl] (**7'**) which were prepared as described for complex **7** in the literature.[15] Single crystals suitable for structure determination by X-ray diffraction were grown by layering a concentrated solution of **7'b** in DCM with MeCN resulting in a pink acetonitrile adduct [Tp$^{Mes}$*Co(NCMe)Cl], **7'b·MeCN**, analogous to the respective iron complex. The cobalt chlorido complexes **7** and **7'** were reacted with cysteamine under similar conditions, as described for complexes **4b** and **4'b**, which yielded the dark red complexes [Tp$^{Mes}$CoCysAm], **8b**, and [Tp$^{Mes}$*CoCysAm], **8'b**. Spectroscopic data largely corresponded to those of the respective iron(II) containing complexes. Single crystals of complex **8b** suitable for X-ray diffraction were grown from toluene and **8b** was found to be isostructural to complex **4b** (see Supporting Information, Figure S3). However, the dark red compound **8b** does not react with dioxygen in acetone, neither at room temperature, nor at low temperatures. [Tp$^{Mes}$*CoCysAm], **8'b**, did also not react with dioxygen under similar conditions at room temperature. However, at low temperatures such as −80 °C **8'b** was converted into a red species (**9'b**) (Figure 8), which is stable for extended periods of

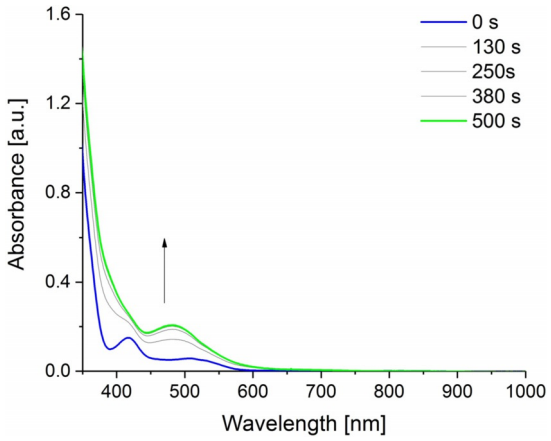


**Figure 8.** UV/Vis spectra illustrating the generation of the intermediate [Tp$^{Mes}$*Co(CysAm)(O$_2^{-\bullet}$)], **9'b**, from [Tp$^{Mes}$*CoCysAm], **8'b**, (0.4 mM) at −80 °C in oxygen saturated acetone.

time without any further reaction. This observation is in consistency with the accumulation of the intermediate **6'b** at low temperatures, which was also only accessible with the asymmetric ligand. The absorbance maxima characteristic of complex **8'b** at 418 and 513 nm change to a more intense absorbance maximum at 482 nm. Oxygen was found to bind reversibly and can be removed by warming up to room temperature or by purging the solution with argon. By purging the cold solution with oxygen, the $O_2$ adduct can be regained. Three cycles of this reversible oxygen binding were performed and monitored by the increase and decrease of the absorption at 482 nm in the electronic spectrum (Figure 9). No further reaction with the thiolate of the bound substrate nor with the solvent was observed. These observations suggest **9'b** to correspond to the superoxide [Tp$^{Mes}$*Co(CysAm)(O$_2^{-\bullet}$)]. To obtain further support for this assignment **9'b** was generated in cold oxygen saturated acetone and an X-band EPR spectrum was recorded. While at 77 K the cobalt(II) precursors **8b** and **8'b**

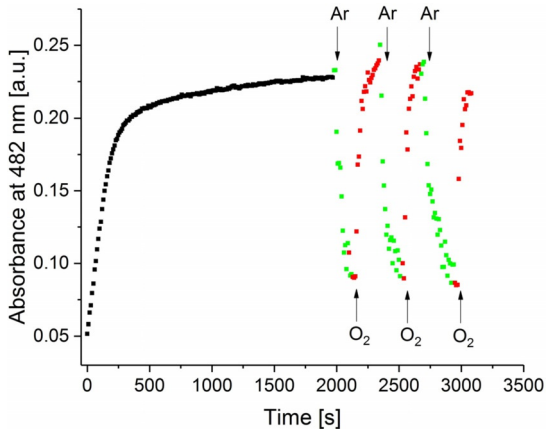


**Figure 9.** Monitoring the absorbance at 482 nm belonging to the electronic spectrum of [Tp$^{Mes}$*Co(CysAm)(O$_2^{-\bullet}$)], **9'b**, formed from [Tp$^{Mes}$*CoCysAm], **8'b**, (0.4 mM) at −80 °C in oxygen saturated acetone and the effects of purging with Ar and $O_2$ gas.

were EPR silent **9'b** showed resonances between 3100 and 3500 mT. The best fit of the data was achieved considering two species, with the first one causing a minor rhombic $S=1/2$ signal without hyperfine coupling ($g_x=2.00$, $g_y=2.04$, $g_z=2.08$), probably caused by free superoxide radical,[30] and a second one leading to a much more intense quasi-axial signal ($g_x=2.00$, $g_y=2.01$, $g_z=2.06$) with clearly resolved hyperfine coupling to the $S=7/2$ nucleus of $^{59}Co$ ($A_z=20.7$ G; see Figures S48 and S49). An end-on cobalt(III) superoxide species, reported in 2017 by Fiedler and co-workers to form in course of $O_2$ treatment of a cobalt(II) precursor [$Tp^{Me2}$CoCysOEt], exhibited an almost identical electronic spectrum as well as a comparable EPR spectrum, and consequently, an assignment of intermediate **9'b** as [$Tp^{Mes}$*Co(CysAm)($O_2^{-\bullet}$)] is reasonable.[31] Goldberg and co-workers just recently published the generation of a $Co^{III}$-superoxide $Co(O_2)(Me_3TACN)(S_2SiMe_2)$ by treating $Co(Me_3TACN)(S_2SiMe_2)$ with dioxygen at $-80\,^{\circ}C$.[32] Also this cobalt complex binds dioxygen (irreversibly) to give a cobalt(III) superoxide species.

### Influence of the Tp ligands

To deconvolute steric and electronic effects of the ligands on the complex reactivities cyclic voltammetry investigations were performed on complexes **1b**, **4b**, **4'b**, **8b** and **8'b** (see Figure 10 and Supporting Information, Figures S40–S47). By comparing the three iron complexes it becomes evident that complex **1b** with the $Tp^{Ph,Me}$ ligand shows a reversible electron transfer coupled with an irreversible consecutive chemical reaction revealed by measurements with variable scan rates between 50 and 400 mV s$^{-1}$ (see Supporting Information, Figure S41).[33] The anodic peak potential $E_{pa}$ appears at $-0.15$ V and the corresponding cathodic peak potential $E_{pc}$ at $-0.26$ V versus the ferrocene ferrocenium redox couple ($Fc/Fc^+$). In

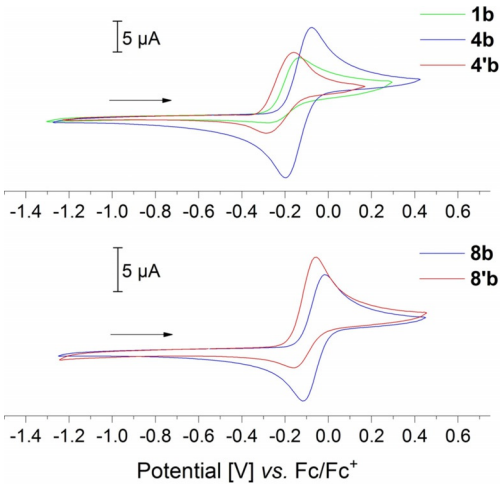


**Figure 10.** Cyclic voltammograms of complexes [$Tp^{Ph,Me}$FeCysAm], **1b** ($E_{pa}=-0.15$ V, $E_{pc}=-0.26$ V), [$Tp^{Mes}$FeCysAm], **4b** ($E_{pa}=-0.08$ V, $E_{pc}=-0.20$ V, $E_{1/2}=-0.14$ V), [$Tp^{Mes*}$FeCysAm], **4'b** ($E_{pa}=-0.18$ V, $E_{pc}=-0.27$ V), $Tp^{Mes}$CoCysAm], **8b** ($E_{pa}=-0.03$ V, $E_{pc}=-0.12$ V, $E_{1/2}=-0.07$ V), [$Tp^{Mes*}$CoCysAm], **8'b** ($E_{pa}=-0.07$ V, $E_{pc}=-0.16$ V), scan rate 100 mV s$^{-1}$ in DCM (100 mM TBAPF, 1 mM complex).

In contrast to this, complex **4b** exhibits a fully reversible cyclic voltammogram with a quotient between $i_{pc}$ and $i_{pa}$ around 1 for all measured scan rates. The $E_{pa}$ is shifted by $-70$ mV to $-0.08$ V and $E_{pc}$ by $-60$ mV to $-0.20$ V versus $Fc/Fc^+$. A lower $E_{pa}$ implies that complex **1b** should be more susceptible to oxidants such as dioxygen, but the opposite is the case. The rather small influence of the Tp ligand on the electronic properties seems to play only a negligible role on reactivity with dioxygen, which underlines the importance of the steric environment around the metal center in the comparison of these two complexes.

In the case of complex **4'b** the position of the mesityl group not only has an influence on the steric conditions but also on the redox potentials, as $E_{pa}$ shifts by 100 mV to $-0.18$ V and $E_{pc}$ by 70 mV to $-0.27$ V versus $Fc/Fc^+$ compared to complex **4b**. Measurements with variable scan rates between 50 and 400 mV s$^{-1}$ show again an increasing quotient $i_{pc}/i_{pa}$ with increasing scan rate, which indicates a reversible electron transfer coupled with an irreversible chemical reaction (see Supporting Information, Figure S44). The mesityl residue in the 5-position is missing within the shield of organic groups protecting the metal center, which makes consecutive side reactions more likely than for complex **4b**. Together with the cyclic voltammograms of complexes **1b** and **4b** no conclusive correlation between redox properties and reaction rate with dioxygen can be found, which in turn again emphasizes the influence of the steric properties of the ligand.

The cyclic voltammograms of the corresponding cobalt complexes are shifted by $-70$ mV in the case of complex **8b** compared to complex **4b** and $-110$ mV in the case of complex **8'b** compared to complex **4'b** (Figure 10). As already observed for the iron(II) complexes the complex with the unsymmetrical ligand **8'b** shows a reversible electron transfer coupled with an irreversible chemical reaction (see Supporting Information, Figure S47) whereas complex **8b** shows only a reversible electron transfer, which is consistent with the results obtained for the iron complexes. The small shift of the $E_{pa}$ caused by the position of the mesityl residue either in 3- or in 5-position cannot explain the fact that superoxo species **6'b** and **9'b** can only be observed with the unsymmetrical ligand $Tp^{Mes}$*. An accumulation of the respective superoxo species seems to be only possible if sufficient space is provided around the metal center. The mesityl residue in 5-position offers this extra space in complexes **4'b** and **8'b**.

## Conclusions

A series of iron(II) complexes with mesityl-substituted tris(pyrazolyl) borate spectator ligands and cysteinate or cysteaminate substrate ligands has been accessed and investigated as models for the CDO and ADO. It turned out that the seemingly minor change from phenyl residues in previous work to mesityl residues as investigated in the present work has massive consequences for the reactivity towards $O_2$. We had envisaged that the increase of steric bulk upon using mesityl residues would lead to a stabilization and thus further characterization of intermediates and/or final products. Indeed, unlike in the

case of the phenyl residues crystallization of the sulfinate product complexes has been achieved using mesityl residues, so that crystal structure analyses could be performed. This has led to the first structural characterization of a sulfinate product with an $\eta^2$-*O*,*O*-binding mode of the sulfinate group that has also been suggested for the enzymatic product complex. Unexpectedly, it has also been found that despite the increase in steric bulk an acceleration of the reaction rates occurs. This can be rationalized with the aid of the solid-state structures: the mesityl units—unlike the phenyl residues—arrange themselves to a cup, providing more space at the metal center as compared to $Tp^{Ph,Me}$ forming counterintuitively a more spacious reaction pocket, although they are bulkier. If this arrangement translates into solution, this explains the higher rates. The hypothesis that also electronic effects could be responsible has been ruled out by means of cyclic voltammetry studies. As consequently the space provided in the reaction pocket determines the reaction rate, it is not surprising that complex **4'b** with one of the mesityl residues in 5-position, offering an even more open pocket, show the highest reaction rates. In the case of **4'b** a reaction intermediate has been identified at low temperatures by UV/Vis and Mössbauer spectroscopy, which through comparison with literature reports and investigations on the cobalt analogues as part of this work is tentatively assigned to an iron(III) superoxide intermediate—the first precedence of such a species where in addition the native substrate cysteamine is bound. In future work, we will try to utilize this knowledge to gain even more information on the mechanism and intermediates through ligand design.

## Experimental Section

### Crystallographic data

Deposition Numbers 1899929, 1899932, 1899934, 1899933, 1899935, 1899931, 1899930, and 1899936 contain the supplementary crystallographic data for this paper. These data are provided free of charge by the joint Cambridge Crystallographic Data Centre and Fachinformationszentrum Karlsruhe Access Structures service www.ccdc.cam.ac.uk/structures.

## *Acknowledgements*

C.L. and L.M. are grateful to the Deutsche Forschungsgemeinschaft (DFG, German Research Foundation) for funding under Germany's Excellence Strategy– EXC 2008 – 390540038 – UniSysCat, as well as the Humboldt-Universität zu Berlin for financial support. Open access funding enabled and organized by Projekt DEAL.

## Conflict of interest

The authors declare no conflict of interest.

**Keywords:** dioxygenases · enzyme models · nonheme iron · reaction intermediates · spectroscopy

[1] a) M. Costas, M. P. Mehn, M. P. Jensen, L. Que, Jr., *Chem. Rev.* **2004**, *104*, 939 – 986; b) P. C. A. Bruijnincx, G. van Koten, R. J. M. Klein Gebbink, *Chem. Soc. Rev.* **2008**, *37*, 2716 – 2744; c) A. R. McDonald, L. Que, Jr., *Coord. Chem. Rev.* **2013**, *257*, 414 – 428; d) K. Ray, F. F. Pfaff, B. Wang, W. Nam, *J. Am. Chem. Soc.* **2014**, *136*, 13942 – 13958; e) H. Nakamura, Y. Matsuda, I. Abe, *Nat. Prod. Rep.* **2018**, *35*, 633 – 645.

[2] a) M. M. Abu-Omar, A. Loaiza, N. Hontzeas, *Chem. Rev.* **2005**, *105*, 2227 – 2252; b) I. Siewert, C. Limberg, *Chem. Eur. J.* **2009**, *15*, 10316 – 10328; c) M. Atanasov, P. Comba, S. Hausberg, B. Martin, *Coord. Chem. Rev.* **2009**, *253*, 2306 – 2314; d) M. Costas, *Coord. Chem. Rev.* **2011**, *255*, 2912 – 2932; e) W. Nam, Y.-M. Lee, S. Fukuzumi, *Acc. Chem. Res.* **2014**, *47*, 1146 – 1154; f) C. Buron, K. Sénéchal-David, R. Ricoux, J.-P. Le Caër, V. Guérineau, P. Méjanelle, R. Guillot, C. Herrero, J.-P. Mahy, F. Banse, *Chem. Eur. J.* **2015**, *21*, 12188 – 12193.

[3] a) A. L. Feig, S. J. Lippard, *Chem. Rev.* **1994**, *94*, 759 – 805; b) E. I. Solomon, T. C. Brunold, M. I. Davis, J. N. Kemsley, S. K. Lee, N. Lehnert, F. Neese, A. J. Skulan, Y. S. Yang, J. Zhou, *Chem. Rev.* **2000**, *100*, 235 – 349; c) *Iron-Containing Enzymes: Versatile Catalysts of Hydroxylation Reactions in Nature* (Eds.: S. P. de Visser, D. Kumar), RSC, Cambridge, **2011**.

[4] a) C. A. Joseph, M. J. Maroney, *Chem. Commun.* **2007**, 3338 – 3349; b) D. Buongiorno, G. D. Straganz, *Coord. Chem. Rev.* **2013**, *257*, 541 – 563.

[5] a) J. E. Dominy, C. R. Simmons, L. L. Hirschberger, J. Hwang, R. M. Coloso, M. H. Stipanuk, *J. Biol. Chem.* **2007**, *282*, 25189 – 25198; b) M. H. Stipanuk, C. R. Simmons, P. A. Karplus, J. E. Dominy, *Amino Acids* **2011**, *41*, 91 – 102; c) M. Fellner, E. Siakkou, A. S. Faponle, E. P. Tchesnokov, S. P. de Visser, S. M. Wilbanks, G. N. L. Jameson, *J. Biol. Inorg. Chem.* **2016**, *21*, 501 – 510; d) S. Ye, X. Wu, L. Wei, D. Tang, P. Sun, M. Bartlam, Z. Rao, *J. Biol. Chem.* **2007**, *282*, 3391 – 3402; e) C. M. Driggers, R. B. Cooley, B. Sankaran, L. L. Hirschberger, M. H. Stipanuk, P. A. Karplus, *J. Mol. Biol.* **2013**, *425*, 3121 – 3136.

[6] a) Y. Jiang, L. R. Widger, G. D. Kasper, M. A. Siegler, D. P. Goldberg, *J. Am. Chem. Soc.* **2010**, *132*, 12214 – 12215; b) A. C. McQuilken, Y. Jiang, M. A. Siegler, D. P. Goldberg, *J. Am. Chem. Soc.* **2012**, *134*, 8758 – 8761; c) D. Kumar, G. N. Sastry, D. P. Goldberg, S. P. de Visser, *J. Phys. Chem. A* **2012**, *116*, 582 – 591.

[7] M. Sallmann, I. Siewert, L. Fohlmeister, C. Limberg, C. Knispel, *Angew. Chem. Int. Ed.* **2012**, *51*, 2234 – 2237; *Angew. Chem.* **2012**, *124*, 2277 – 2280.

[8] M. Sallmann, S. Kumar, P. Chernev, J. Nehrkorn, A. Schnegg, D. Kumar, H. Dau, C. Limberg, S. P. de Visser, *Chem. Eur. J.* **2015**, *21*, 7470 – 7479.

[9] a) G. Villar-Acevedo, P. Lugo-Mas, M. N. Blakely, J. A. Rees, A. S. Ganas, E. M. Hanada, W. Kaminsky, J. A. Kovacs, *J. Am. Chem. Soc.* **2017**, *139*, 119 – 129; b) A. A. Fischer, S. V. Lindeman, A. T. Fiedler, *Chem. Commun.* **2018**, *54*, 11344 – 11347; c) K. Anandababu, R. Ramasubramanian, H. Wadepohl, P. Comba, N. Johnee Britton, M. Jaccob, R. Mayilmurugan, *Chem. Eur. J.* **2019**, *25*, 9540 – 9547.

[10] M. Sallmann, C. Limberg, *Acc. Chem. Res.* **2015**, *48*, 2734 – 2743.

[11] M. Sallmann, F. Oldenburg, B. Braun, M. Réglier, A. J. Simaan, C. Limberg, *Angew. Chem. Int. Ed.* **2015**, *54*, 12325 – 12328; *Angew. Chem.* **2015**, *127*, 12501 – 12505.

[12] I. Siewert, C. Limberg, *Angew. Chem. Int. Ed.* **2008**, *47*, 7953 – 7956; *Angew. Chem.* **2008**, *120*, 8071 – 8074.

[13] a) S. Aluri, S. P. de Visser, *J. Am. Chem. Soc.* **2007**, *129*, 14846 – 14847; b) D. Kumar, W. Thiel, S. P. de Visser, *J. Am. Chem. Soc.* **2011**, *133*, 3869 – 3882; c) A. S. Faponle, F. P. Seebeck, S. P. de Visser, *J. Am. Chem. Soc.* **2017**, *139*, 9259 – 9270.

[14] A. L. Rheingold, C. B. White, S. Trofimenko, *Inorg. Chem.* **1993**, *32*, 3471 – 3477.

[15] R. J.-C. Dubey, R. J. Comito, Z. Wu, G. Zhang, A. J. Rieth, C. H. Hendon, J. T. Miller, M. Dincă, *J. Am. Chem. Soc.* **2017**, *139*, 12664 – 12669.

[16] F. A. Kunrath, R. F. De Souza, O. L. Casagrande, N. R. Brooks, V. G. Young, *Organometallics* **2003**, *22*, 4739 – 4743.

[17] M. Sallmann, B. Braun, C. Limberg, *Chem. Commun.* **2015**, *51*, 6785 – 6787.

[18] T. Tietz, C. Limberg, R. Stößer, B. Ziemer, *Chem. Eur. J.* **2011**, *17*, 10010 – 10020.

[19] L. Falivene, Z. Cao, A. Petta, L. Serra, A. Poater, R. Oliva, V. Scarano, L. Cavallo, *Nat. Chem.* **2019**, *11*, 872 – 879.

[20] A. A. Fischer, N. Stracey, S. V. Lindeman, T. C. Brunold, A. T. Fiedler, *Inorg. Chem.* **2016**, *55*, 11839 – 11853.

[21] J. B. Gordon, J. P. McGale, J. R. Prendergast, Z. Shirani-Sarmazeh, M. A. Siegler, G. N. L. Jameson, D. P. Goldberg, *J. Am. Chem. Soc.* **2018**, *140*, 14807 – 14822.
[22] E. Lindner, G. Vitzthum, *Chem. Ber.* **1969**, *102*, 4053 – 4061.
[23] E. Lindner, G. Vitzthum, *Chem. Ber.* **1969**, *102*, 4062 – 4069.
[24] E. P. Tchesnokov, A. S. Faponle, C. G. Davies, M. G. Quesne, R. Turner, M. Fellner, R. J. Souness, S. M. Wilbanks, S. P. de Visser, G. N. L. Jameson, *Chem. Commun.* **2016**, *52*, 8814 – 8817.
[25] M. N. Blakely, M. A. Dedushko, P. C. Yan Poon, G. Villar-Acevedo, J. A. Kovacs, *J. Am. Chem. Soc.* **2019**, *141*, 1867.
[26] F. Oddon, Y. Chiba, J. Nakazawa, T. Ohta, T. Ogura, S. Hikichi, *Angew. Chem. Int. Ed.* **2015**, *54*, 7336 – 7339; *Angew. Chem.* **2015**, *127*, 7444 – 7447.
[27] E. Münck, *Physical Methods in Bioinorganic Chemistry* (Ed.: L. Que, Jr.), University Science Books, Sausalito, **2000**, pp. 287 – 319.
[28] C.-W. Chiang, S. T. Kleespies, H. D. Stout, K. K. Meier, P.-Y. Li, E. L. Bominaar, L. Que, Jr., E. Münck, W.-Z. Lee, *J. Am. Chem. Soc.* **2014**, *136*, 10846 – 10849.
[29] S. Hong, K. D. Sutherlin, J. Park, E. Kwon, M. A. Siegler, E. I. Solomon, W. Nam, *Nat. Commun.* **2014**, *5*, 5440.
[30] R. N. Bagchi, M. Bond, F. Scholz, R. Stösser, *J. Am. Chem. Soc.* **1989**, *111*, 8270 – 8271.
[31] A. A. Fischer, S. V. Lindeman, A. T. Fiedler, *Dalton Trans.* **2017**, *46*, 13229 – 13241.
[32] J. B. Gordon, A. C. Vilbert, M. A. Siegler, K. M. Lancaster, P. Moënne-Loccoz, D. P. Goldberg, *J. Am. Chem. Soc.* **2019**, *141*, 3641 – 3653.
[33] N. Elgrishi, K. J. Rountree, B. D. McCarthy, E. S. Rountree, T. T. Eisenhart, J. L. Dempsey, *J. Chem. Educ.* **2018**, *95*, 197 – 206.

Manuscript received: April 15, 2020
Accepted manuscript online: May 20, 2020
Version of record online: August 13, 2020